The Deelen Infrasound Array: on the detection and identification of infrasound

L.G. Evers and Dr. H.W. Haak

KNMI Technical Report (TR) - 225
ISBN: 90-369-2175-9
August 2000

Royal Netherlands Meteorological Institute
Seismology Division

Contents

1 Samenvatting (in Dutch)

De afdeling Seismologie van het KNMI beschikt sinds 1999 over het operationele Deelen Infrasound Array (DIA). DIA is het resultaat van het KNTP (Kortlopend Nationaal Technologie Project) N98/32 "Sonic Boom Detectie Tecnhiek" uitgevoerd in opdracht van de Koninklijke Luchtmacht (KLu). Het ontwerp van DIA is gebaseerd op de volgende doelstellingen:
1. een techniek ontwikkelen om sonic booms te registreren
2. het demonstreren van de techniek aan de hand van een array van druksensoren op vliegbasis Deelen
3. de KLu en het publiek informatie verschaffen en om de afhandeling van schade claims ten gevolge van sonic booms gemakkelijker te maken.
DIA wordt tevens ingezet als experimenteel array voor onderzoek betreffende wetenschappelijke ontwikkelingen gerelateerd aan het kernstopverdrag (Comprehensive Nuclear-Test-Ban Treaty - CTBT). Om bovenstaande doelstellingen te realiseren heeft de afdeling Seismologie van het KNMI, de volgende onderzoeks- en ontwikkelingsinspanningen geleverd. Om laag frequent geluid te kunnen meten in een robuuste veldtoepassing is de KNMI microbarograaf ontwikkeld. Deze microbarograaf bestaat onder andere uit een differentiële drukopnemer die, gekoppeld aan poreuze slang als windruisonderdrukker, drukvariaties tussen de 0.002 en 30 Hz meet. Op vliegbasis Deelen zijn zestien microbarografen geinstalleerd. De configuratie van de instrumenten is dusdanig dat het array de atmosfeer in iedere riching op gelijke wijze bemonsterd. Ofwel, de gevoeligheid van het array is onafhankelijk van de invalshoek van het geluid. Op basis van digitale array signaalverwerkingstechnieken wordt signaal detectie en lokalisatie uitgevoerd. Zowel tijd- als frequentiedomein, in combinatie met Fisher statistiek, analyse leidt tot een nauwkeurige detectie van infrageluid. Een kruispeiling met gegevens van twee experimentele array's in de Bilt en Witteveen, geeft de lokatie van de bron. Andere bronnen die infrageluid genereren zijn onder andere: explosies, staande golven in de oceaan en exploderende meteoren. De gevoeligheid en resolutie van DIA wordt ook geillustreerd aan de hand van een gedetecteerde meteoor explosie boven Noord Duitsland.

Dit rapport beschrijft de bevindingen, ontwikkelingen en het onderzoek, gedaan om DIA te realiseren. Tevens worden werkzaamheden op het gebied van infrasound in het algemeen beschreven.

2 Summary

The Seismology Division of the Royal Netherlands Meteorological Institute (KNMI) operates since 1999 the Deelen Infrasound Array. DIA is the outcome of a KNTP (Kortlopend Nationaal Technologie Project) N98/32 "Sonic Boom Detection Technique" executed for the Royal Netherlands Airforce (KLu). The design of DIA is based on the following objectives:
1. develop a technique to record sonic booms
2. demonstrate the technique by installing an array of pressure sensors on Airforce base Deelen
3. enable the KNMI to assist the KLu in handling damage claims from sonic booms and to provide public information.
DIA also acts as experimental array for Comprehensive Nuclear-Test-Ban Treaty (CTBT) related issues. The KNMI micro-barometer was developed to detect infrasound generated by amongst others sonic booms. A differential pressure sensor is the infrasound sensitive element of the micro-barometer. Porous hoses are coupled to each instrument to reduce wind noise. Doing so, pressure variations between 0.002 and 30 Hz can be measured. Sixteen micro-barometers are installed on Airforce base Deelen. Sampling the atmosphere in a homogeneous way is the main criterion for the array design. The sensitivity of the optimal array is independent of the azimuth of the incoming infrasonic energy. Array processing techniques are used to detect and localize infrasound. Time and frequency domain analyses, combined with Fisher statistics enable an clear detection of infrasound. Localization is achieved through cross-bearing with data from two experimental arrays in De Bilt and Witteveen. Infrasound is also generated by: explosions, standing wave patterns in the ocean and exploding meteors. The sensitivity and resolutional properties of DIA are illustrated with the recording of an exploding meteor above Northern Germany.

This report describes the research and development done to realize DIA. Furthermore, the work done in infrasound is described.

3 Introduction

The Seismology Division of the Royal Netherlands Meteorological Institute (KNMI) started measuring low frequency sound (infrasound) in 1985. Infrasound are pressure variations in the atmosphere with frequencies varying between 0.002 and 30 Hz. Figure 3.1 shows the recording of an acoustic event on a seismometer. The motivation for measuring infrasound is to distinguish these acoustic events from earthquakes. It became clear that a signal as displayed in figure 3.1, is caused by fighter planes crossing the sound barrier.

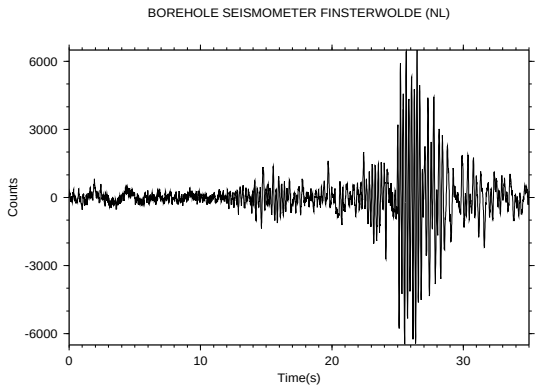

Figure 3.1: *An acoustic event on a seismometer*

Infrasound measurements have been selected within the Comprehensive Nuclear-Test-Ban Treaty (CTBT) as a technique to detect and identify possible nuclear explosions. For this purpose, a world-wide network of 60 infrasound stations is presently being constructed (*PrepCom,* 1997).
Based on the experience gained in measuring and analyzing infrasound, the Royal Netherlands Air force (KLu) asked the KNMI to execute a KNTP (Kortlopend Nationaal Techniek Project) on "Sonic Boom Detection Technique". The goals of the KNTP N98/32 were:
1 development of a robust technique in order to properly record sonic booms
2 demonstrate an array of pressure sensors at the Air force base in Deelen
3 enable the KNMI to assist the KLu in handling damage claims from sonic booms and to provide public information.
In order to meet objectives, the Deelen Infrasound Array (DIA) was developed. DIA is capable of detecting sonic booms and events of CTBT interest. DIA is not part of the CTBT network, but acts as an experimental array for CTBT related topics.
Detecting infrasound can be achieved by making a microphone sensitive for low frequencies or a barograph for higher frequencies. We choose the latter approach for constructional and durability reasons. Chapter 4 describes the development of the so-called KNMI micro-barometer. An array of instruments can localize infrasound on the basis of signal coherency. An optimal array will unambiguously detect and localize infrasonic energy by spatially sampling the surrounding atmosphere, as described in chapter 5. Array processing techniques as known from seismology are used to handle the data and to develop a low threshold detector based on Fisher statistics. In chapter 6 frequency domain processing is explained and its use is exemplified by a sonic boom detection and recordings from an exploding meteor.

4 The KNMI micro-barometer

Pressure variations can be measured absolutely or differentially, i.e. with respect to a reference pressure. Although, the need for a constant reference pressure introduces a strong temperature dependency, we choose for a differential micro-barometer since it is far more easy to tune. The KNMI micro-barometer, shown in figure 4.1, was developed. While constructing the instrument, two fundamental characteristics had to be fulfilled. (1) The ability of the instrument to record events in the infrasonic spectrum. (2) A robust construction for durable operation in the field.

4.1 Structural properties

Several elements can be distinguished in figure 4.1 (for a detailed constructional drawing

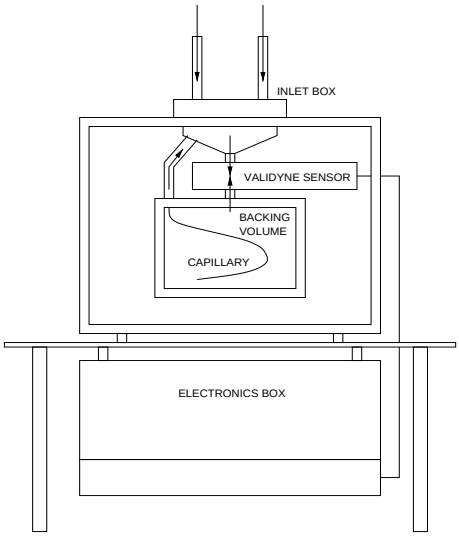

Figure 4.1: *Schematic view of the KNMI micro-barometer*

see Appendix A). The two vertical pipes, at the top, are part of a system of six inlets connecting the atmosphere to the inlet box. The small volumes assure having a high resonance frequency (i.e. higher than 40 Hz) outside the spectrum of interest. A pressure wave is guided, through the inlets, to the sensor. Recording in the infrasonic spectrum implies measuring low frequency variations in the atmosphere. Validyne Engineering Corp. has developed differential pressure sensors for, amongst others, these purposes. The device has a resonance frequency of 1500 Hz, thus outside of the spectrum of interest. Since the Validyne device measures differential, i.e. with respect to a constant pressure, a backing volume is connected beneath it. The thick walled aluminum construction of the backing volume guarantees a stable temperature within the volume, essential for a constant pressure. The KNMI micro-barometer would also be able to measure very low frequent pressure variations, like meteorological phenomena, if no "leak" was enclosed in the instrument. Within the backing volume a thin capillary is used to suppress these effects. Through its connection to the open air and characteristic acoustical resistance, very low frequent signal is filtered from the recordings. The electronics are placed in a box beneath the instrument. They consist of a CD101 single channel carrier Demodulator (Validyne Engineering Corp. and a DC/DC converter.

4.2 Operating principles of the Validyne sensor

Validyne sensors have the ability to measure low pressures accurately, with rugged durability (p.e. non corrosive). This is achieved by making no connections or linkages to the sensing element with the transducer, based on variable reluctance pressure sensing technology. Figure 4.2 displays the so-called inductive half-bridge, consisting of a pressure

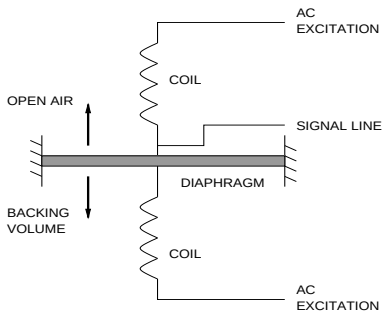

Figure 4.2: *Variable reluctance circuit*

sensing diaphragm and two coils. The coils are wired in series, vertically to the diaphragm. Clamped between the coil housings, the flexible diaphragm is free to move in response to differential pressure. The two coils are matched, so their impedances are approximately equal. The coils are supplied with an AC excitation to create a magnetic flux. Deflection of the magnetic permeable diaphragm, due to differential pressure, will increase the magnetic flux density of the approached coil. The stronger magnetic field of the coil, in turn, causes its inductance to increases the impedance of that coil. The change in coil impedance brings the half-bridge out of balance, a small AC signal appears on the signal line. The change in coil impedance is directly proportional to the position of the diaphragm, so the amplitude of the signal is directly proportional to the applied pressure. The phase of the signal is determined by the direction of movement of the diaphragm. In

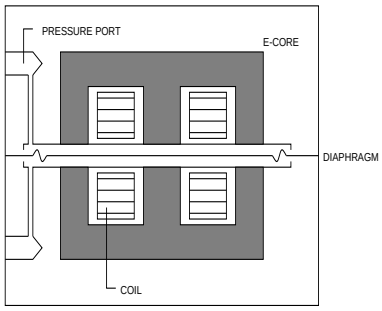

Figure 4.3: *Transducer cross section*

figure 4.3, the inclusion of the variable reluctance circuit within the pressure transducer is shown. The coils are enclosed within two e-cores. As a result of this, the diaphragm has to be accelerated and moved but a small distance to reflect a change in pressure.

4.3 Response characteristics

As described, a thin capillary is placed within the backing volume to suppress very low frequent pressure variations. The capillary controls the low frequency cut-off, f_l, of the

instrument. The low frequency cut-off is the lowest frequency which can be measured. Atmospheric pressure variations with a lower frequency than f_l will be guided back to the open air through the capillary.
The relaxation of the diaphragm induced by suddenly over-pressuring or expanding air within the instruments volumes, is described by (*Haak and de Wilde,* 1996):

$$\frac{P_t}{P_0} = \frac{V_t}{V_0} = e^{-\alpha t} \tag{4.1}$$

In formula 4.1 the over-pressured starting situation, P_0, is relaxated by the diaphragm in time, t. Within the sensor, pressure variations, P_t, are directly proportional to voltage variations, V_t. The capillary controls the time necessary to reach an equilibrium between open air and backing volume pressure by a constant, α.
The relaxation time, τ, is defined as the time necessary to let amplitude, i.e. voltage, decay to e^{-1}. This is also known as -3dB cut off, thus:

$$e^{-\alpha\tau} = e^{-1}, \alpha = f_l = \frac{1}{2\pi\tau} \tag{4.2}$$

Equation 4.1 implies the following experiment. All inlets are closed, by suddenly opening one of the inlets, the relaxation time can be measured. An identical experiment would be the sudden closure of all inlets, after which the relaxation time can be measured. This reversed experiment will lead to the same voltage values, with reversed signal phase.

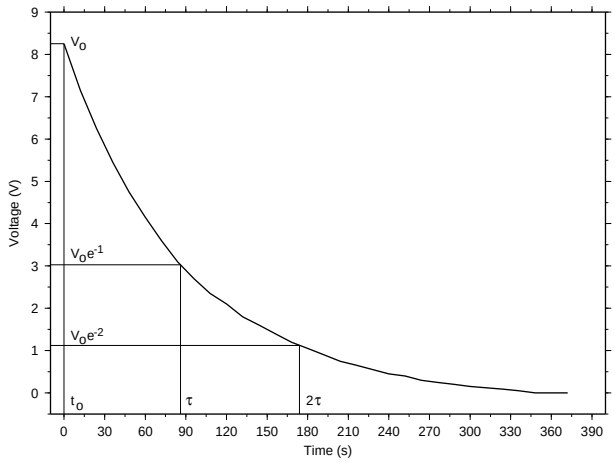

Figure 4.4: *Low frequency cut-off response measurement*

Figure 4.4 shows the results for the relaxation experiment. By making use of equation 4.2, the low cut-off frequency is calculated:

$$f_l = \frac{1}{2\pi 86} \approx \frac{1}{\pi 174} = 1.84 \times 10^{-03} \pm 0.01 \times 10^{-03} Hz \tag{4.3}$$

The low cut-off frequency can easily be tuned, by changing the acoustical resistance of the capillary. A longer capillary or a smaller diameter will increase the acoustical resistance, which lowers f_l.
To measure the total response of the instrument is more difficult. One must be able to generate pressure variations over the frequency range 0.002 to 30 Hz. Furthermore, one must know the absolute values of the applied pressure to be able to calibrate the

instrument. Measurements were conducted to make sure that there were no resonances in the instrument within the mentioned frequency band. This guarantees a flat response of the instrument with respect to frequencies of interest. Thus, the instrument outputs the same differential pressure value, for any identical absolute applied pressure value with variable frequency (between 0.002 and 30 Hz). A flat response will enable a straight forward comparison of recordings, after calibration. A simple calibration experiment, described in Appendix B, was conducted to get an impression of Volts versus pressure values.

4.4 Field setup

The KNMI micro-barometer needs to be placed in a temperature stable environment, since differential pressures are measured. Furthermore, military activity on Airforce Base Deelen implies a firm protection for the instruments. Also, wind generated noise is less near the ground than higher up in the air. The instruments were therefore placed beneath the surface in a pvc tube covered by a concrete top. A cross section of the field setup is shown in figure 4.5. To make sure that the backing volume won't warm up or cool down following temperature fluctuations in the infrasonic band, extra thermal insulation material is placed within the pvc tube.

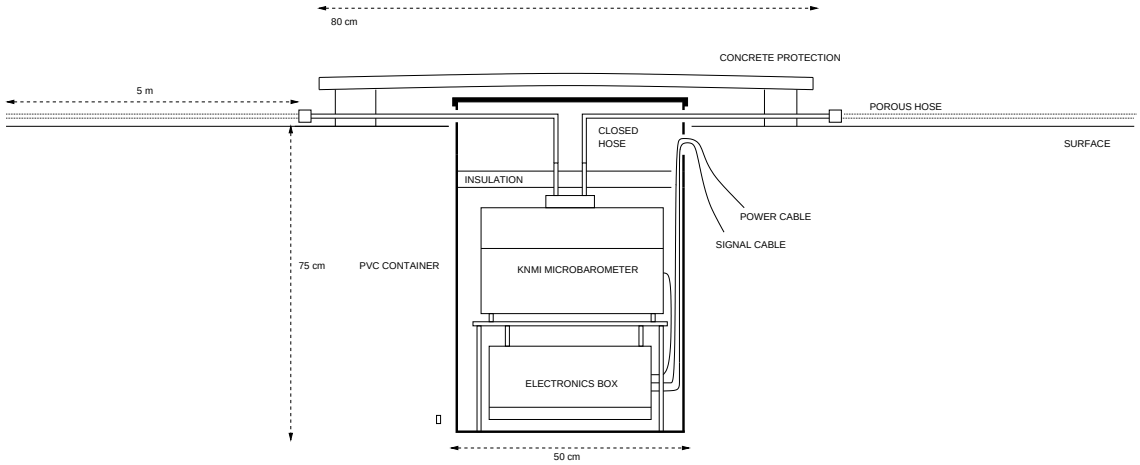

Figure 4.5: *Field setup of KNMI micro-barometer*

4.5 Noise reducers

Wind generates pressure variations with a frequency contents of 0.01 up to 30 Hz. Thus, the signal to noise ratio will severely decrease since infrasonic events appear in the same frequency band. Coherency of both signal and noise is used to reduce noise. Infrasonic signals are coherent over large lengths (kilometers), while wind is only coherent on a smaller scale. By sampling atmospheric pressure over an area rather than one point, uncorrelated noise will be suppressed. This analog filtering is done through the use of porous hoses. Porous hoses are connected to each of the six inlets (see figure 4.5). The size of noise reducers is limited to half the wave-length of the highest frequency of interest. A symmetric star-like layout of six porous hoses with each a length of 5 meters is used. This results in a highest recovered frequency of approximately 30 Hz.

5 Deelen Infrasound Array design

In general, an array is a number of instruments which is, through its lay-out, able to detect signals and localize the incoming direction and angle of the source. The array configuration controls the resolution of the array. An array with optimal resolution is equally sensitive to all infrasonic signals, independent of incoming angle and direction. In other words, the array is capable of homogeneously sampling the surrounding atmosphere.
Array design and calculations are based on signal coherency (*Haak,* 1996). As an incoming wave travels over the instruments, it's assumed that the wavefront has a flat shape (so-called plane wave). In mathematical form, this elementary wave is represented by:

$$f(\mathbf{r},t) = e^{i(\omega t - \mathbf{k}\cdot\mathbf{r})} \tag{5.1}$$

with: frequency ω, travel-time t, wavenumber $\mathbf{k}$ and position $\mathbf{r}$.
Alternatively, the elementary wave can be described as a function of slowness, $\mathbf{p}$, instead of wavenumber, $\mathbf{k}$. With, $\mathbf{p} = \mathbf{k}/\omega$, equation 5.1 becomes:

$$f(\mathbf{r},t) = e^{i\omega(t - \mathbf{p}\cdot\mathbf{r})} \tag{5.2}$$

The design of an array is based on equation 5.2. By letting a plane wave vertically incident on the array, the array response can be modeled. Differential times are zero since the wave is vertically incident and thus recorded at the same time in each instrument. The array response reflects the sensitivity and resolution of the array. The response of an array of N instruments is described by:

$$R(\omega,\mathbf{p}) = \frac{1}{N}\left|\sum_{j=1}^{N} e^{-i\omega(\mathbf{p}\cdot\mathbf{r}_j)}\right|^2 \tag{5.3}$$

The sampling of the atmosphere is controlled by slowness $\mathbf{p}$ in formula 5.3. By adequately choosing the $\mathbf{p}$-space, all coherent energy within the infrasonic spectrum can be modeled. The result for a vertical incident plane wave of frequency 0.1 Hz is shown in figure 5.1. The

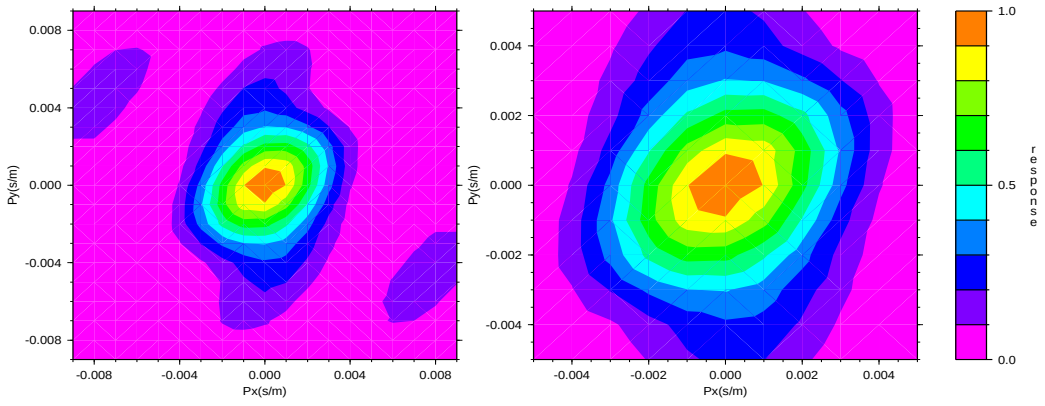

Figure 5.1: *Array response*

array response on the left, in figure 5.1, represents the total space in which infrasonic signal can appear. The right figure is a zoom-in to have a closer look at the array response. The array response has a circular shape. This means that the array has an equal resolution in

all directions. Furthermore, it becomes clear that only one centralized major response is present. Thus, the capability of the array to resolve the source of infrasonic signal is high. If larger so-called side lobes would be present, localization of a source would become less unique since energy would be smeared out.

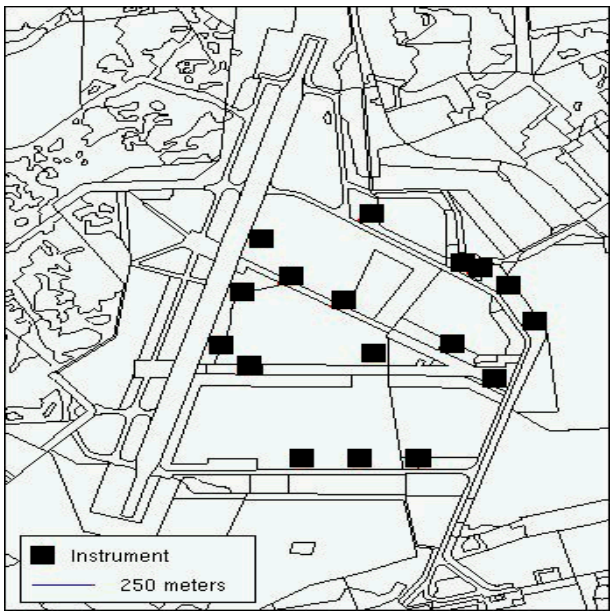

Figure 5.2: *The Deelen array lay-out*

The array lay-out corresponding to the shown response is displayed in figure 5.2, see Appendix C for exact coordinates. This an optimal array lay-out. Optimal with respect to sensitivity and resolution but also optimal when taking into account practical considerations. Practical considerations consist of the presence of trees, buildings etc. Furthermore, human activities (e.g. military and agricultural) in the presence of the infrasound array needed special attention when configuring the lay-out.

6 Data processing

6.1 Signal detection

In general, signal detection can be achieved in the time or frequency domain (*Smart and Flinn,* 1971). The advantages of frequency domain based analysis are: (1) the detection threshold can be lowered by applying statistical methods like Fisher statistics. A Fisher detector also outputs the statistical distribution of the likelihood for signal detection. This means, it is possible to assign a quantitative measure of reliability to each signal pick. (2) Frequency variations of signal arrival azimuth and phase velocity can be taken into account. Frequency-wavenumber (f-k) spectral estimation separates propagating wave components from one another, unlike conventional summation techniques in the time domain (*Cansi,* 1995).
The Fourier transform $A(\omega)$ can be used to convert data $U(t)$, which are measured in the time domain (t) by the j-th instrument, to the frequency domain (ω) through Fourier coefficients $U(\omega)$.

$$A_j(\omega) = \int_{-\infty}^{\infty} U(t) e^{-i\omega t} dt \approx \sum_{j=-\infty}^{\infty} U_j(\omega) e^{i\alpha_j(\omega)} \tag{6.1}$$

where, $\alpha_j(\omega) = -\omega_j t$. The frequency-wavenumber spectrum of the data is defined as:

$$P(\omega, \mathbf{k}) = \sum_{j=1}^{N} \sum_{m=1}^{N} S_{jm}(\omega) e^{[i\mathbf{k}\cdot(\mathbf{r}_j - \mathbf{r}_m)]} \tag{6.2}$$

with: $\mathbf{k}$ as wavenumber, N number of instruments and $\mathbf{r}_{j,m}$ position vector to the j or m-th instrument. In formula 6.2 the frequency domain conversion is denoted by the cross-spectrum S_{jm}, which is a multiplication of the Fourier spectra:

$$S_{jm} = U_j(\omega) e^{-i\alpha_j(\omega)} \cdot U_m(\omega) e^{i\alpha_m(\omega)} \tag{6.3}$$

To reduce the number of computational steps, formula 6.2 can be rewritten to a single summation. This results in the following formula for the frequency-slowness spectrum by making use of $\mathbf{p} = \mathbf{k}/\omega$:

$$P(\omega, \mathbf{p}) = \left| \sum_{n=1}^{N} U_n(\omega) e^{i\alpha(\omega)} \cdot e^{-i\omega \mathbf{p}\cdot\mathbf{r}_n} \right|^2 \tag{6.4}$$

The f-p spectrum $P(\omega, \mathbf{p})$ can be interpreted as a set of beams sampling the atmosphere above the array. The beams are controlled by the slowness $\mathbf{p}$, enabling tuning of the density of beamforming and azimuthal coverage. Coherent energy can be detected, as energy originating from a specific direction in the atmosphere. In this case, the power of the spectrum will increase. The associated best-beam will lead to a detected signal. The beamforming calculations are done over the whole range of frequencies of interest, i.e. 0.002 up to 30 Hz.
Having obtained maxima for the spectral power in the f-p domain, significance of each associated arrival can be computed by the Fisher statistics. The Fisher statistics are defined as:

$$S_F(\omega, \mathbf{p}) = \frac{E(\omega, \mathbf{p})}{E(\omega) - E(\omega, \mathbf{p})} \cdot (N - 1) \tag{6.5}$$

where

$$E(\omega, \mathbf{p}) = \left| \frac{1}{N} \sum_{j=1}^{N} A_j(\omega) e^{-i\omega \mathbf{p} \cdot \mathbf{r}_j} \right|^2 \tag{6.6}$$

$$E(\omega) = \frac{1}{N} \sum_{j=1}^{N} |A_j(\omega)|^2 \tag{6.7}$$

$E(\omega, \mathbf{p})$ represents the spectral amount of energy belonging to signal. This signal power can be obtained from the power spectrum $P(\omega, \mathbf{p})$. The total amount of spectral power, including both noise and signal, is described by $E(\omega)$. Thus, without the $(N-1)$ weighting factor, the Fisher statistics are a measure of the signal-to-noise ratio.
Signal detection is done on the basis of the Fisher statistics for a beam with maximum power, the best-beam. The threshold value for signal detection highly depends on the amount of correlated signal in the time domain or coherent spectral energy in the frequency domain. Signal is detected for values of the Fisher statistics larger than 4.
As described, a best beam is characterized by its frequency and wavenumber. From these values apparent sound velocity of the incoming wave and azimuth from the array to the source, i.e. sonic boom, can be calculated. Having the elementary wave representation:

$$f(\mathbf{r}, t) = e^{i\omega(t - \mathbf{p} \cdot \mathbf{r})} \tag{6.8}$$

than, the slowness vector will resolve both apparent sound velocity c and azimuth ϕ:

$$|\mathbf{p}| = \sqrt{p_x^2 + p_y^2} = \sqrt{(\frac{\cos\phi}{c})^2 + (\frac{\sin\phi}{c})^2} = \frac{1}{c} \tag{6.9}$$

6.2 A sonic boom record

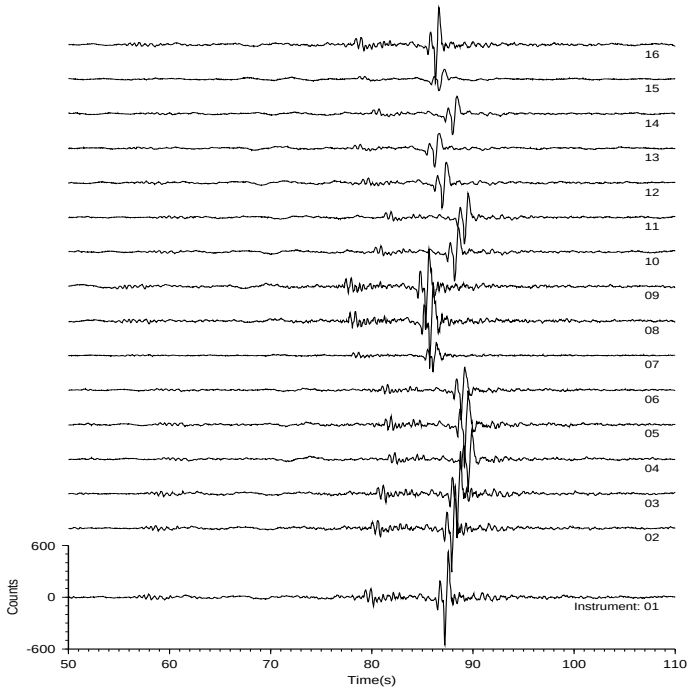

Figure 6.1: *Sonic boom recordings*

Figure 6.1 shows the recording of a infrasonic event. The time axis represents the time on July 07, 1999 since 20h59m19s. The signal travels coherently over the array and the observed differential traveltimes and amplitudes will be used in the time domain to locate the energy. Similarly, corresponding phase differences and amplitudes will resolve event characteristics in frequency domain processing.

6.2.1 Time domain

An approximation of the event origin can be modeled in the time domain. The first arrival is picked in each trace. The absolute recording time of this arrival is used to do a time domain event search. Each arrival time is forwardly modeled for various incoming angles and velocities. The measured and modeled arrival times are compared in least squares sense. Thus, the best obtainable event characteristics are those for which:

$$S(c,\phi) = \sum [t_{measured}(c,\phi) - t_{modeled}(c,\phi)]^2 \tag{6.10}$$

is minimum. In equation 6.10 apparent sound velocity is denoted by c, azimuth by ϕ and least squares by S summed over the number of forward modeling steps. The result of the forward time domain modeling, least squares, compared with the picked times, is shown in figure 6.2. The minimum of formula 6.10 is clearly visible in the center of the plot, where the least squares are close to zero. A estimation of event characteristics gives 322 degrees for the incoming angle and an apparent velocity of 346 m/s. The variance of the minimum is controlled by the uncertainties in time picking, array response and the assumption of a plane wave. In figure 6.3, the traces are aligned with respect to the first instrument which

recorded the event, i.e. instrument 09, using the 346 m/s apparent velocity following from the forward modeling. Doing so, instrument 04 is the last to record the event at a distance of 1500 meters from instrument 09 with respect to the direction of 322 degrees of the incoming sound wave.

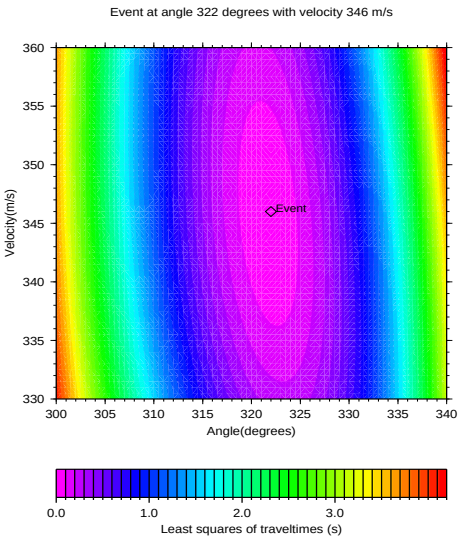

Figure 6.2: *Time domain event search*

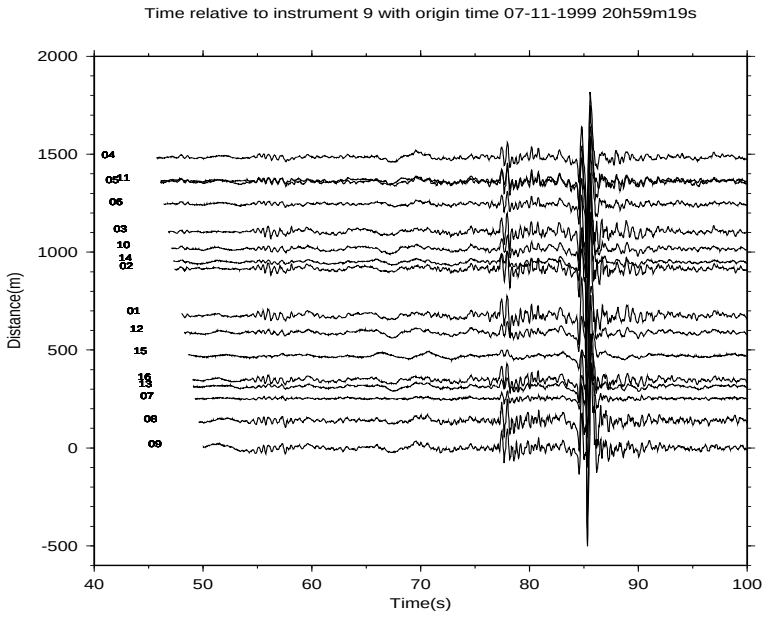

Figure 6.3: *Aligned sonic boom recording*

The described method involves phase picking and therefore a clear first arrival is necessary. Since this is not often the case with infrasonic signals, an automated procedure in the frequency domain will be described.

6.2.2 Frequency domain

As described by formula 6.5, event detection is done on the basis of Fisher statistics. The value of the Fisher statistic is a measure of coherency of the signal. Uncorrelated recordings, like noise, have Fisher values between 0 and 4. Coherent energy has larger Fisher values. The larger the value, the more coherent the signal is, since the signal-to-noise ratio increases. This can be in both displacement as well as time. Thus, small amplitude but in time continuously present signal add up to high Fisher values. On the other hand, a sonic boom which is peaked in time with high amplitude, also adds up to a large Fisher value. Figure 6.4 displays the best beam in its top frame. The best beam is the beam for which the source of infrasonic signal is located with the best resolution. Or, the best beam is the beam for which the fp analyses has the largest power. The best beam is calculated for the sonic boom. The Fisher values are plotted in the lower frame as a function of frequency and time. The time axes in the lower frame corresponds to the time axes for the best beam. In the lower two frames velocity (m/s) and angle (degrees) are plotted.
The best beam is a stack of each individual recording, shown in figure 6.3. Noise, for example due to wind, is clearly uncorrelated since the signal to noise ratio of the stack has increased compared to the individual recordings.

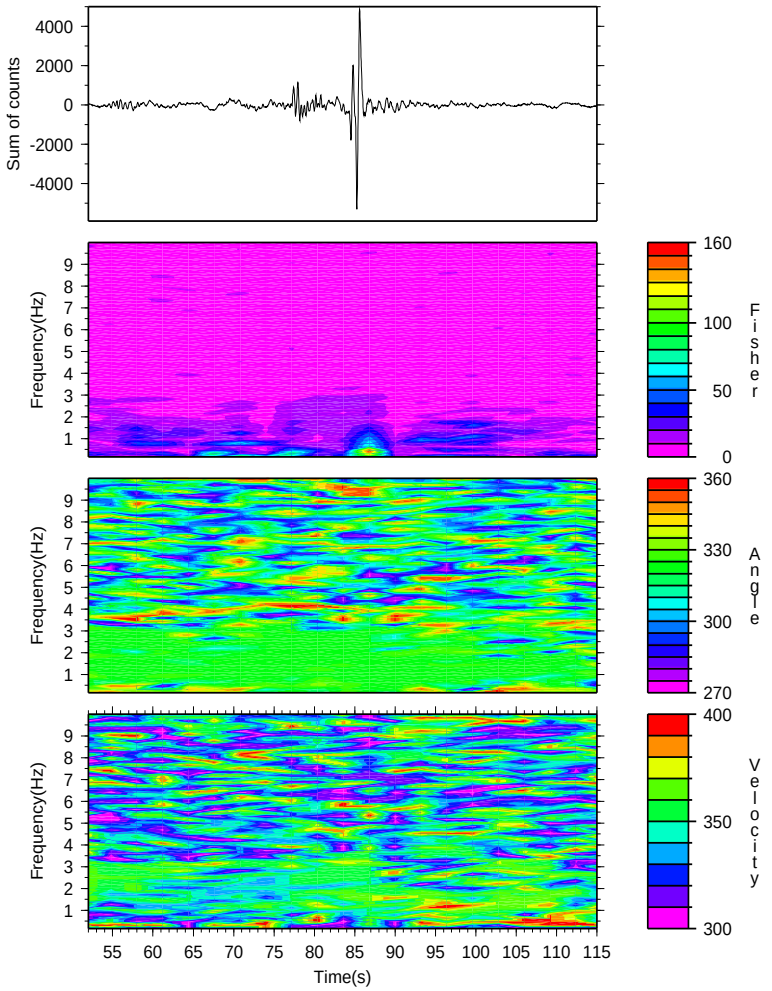

Figure 6.4: *The best beam and characteristic values*

As follows from the Fisher values, coherent energy is present throughout the recording between 0 an 3 Hz. The major peak after 85 seconds results in the highest Fisher value due to its high amplitude and preserved waveform while traveling over the array. Both before and after this arrival coherent energy can be found. Since the energy also stacks up positively in the best beam it's likely to have come from the same direction. The coherency of the signal is also reflected when evaluating the incoming angle of the energy. The light green colored band between 0 and 3 Hz indicates that the energy is coming from a North-western angle with respect to the array. Although the velocity in the lower frame seems less well resolved, lobes of light green colors correspond to reasonable apparent sound velocities.

Exactly locating the sonic boom can be done by evaluating the power of the frequency-slowness spectrum $P(\omega, \mathbf{p})$. As can been seen in figure 6.4, maximum coherency is found around 0.5 Hz at 85 seconds. The normalized values of $P(\omega, \mathbf{p})$ are displayed in figure 6.5 for the 0.5 Hz component of the signal. The phase differences of the traveling

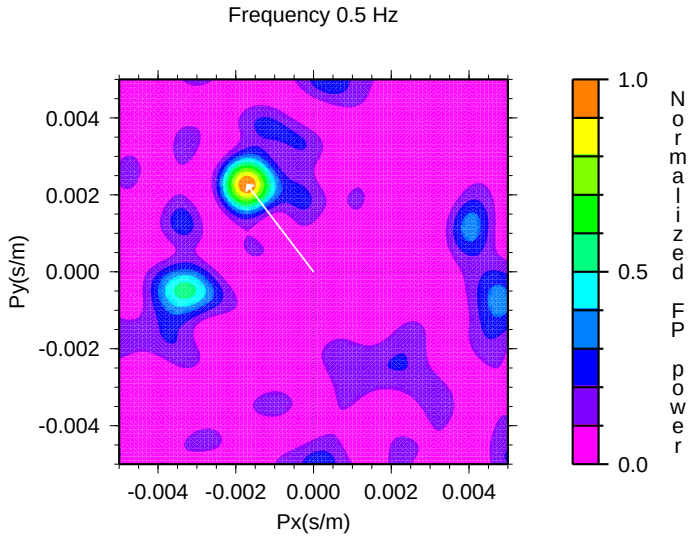

Figure 6.5: *Frequency-slowness analysis*

wave over the array shifts the array response to the North-western quadrant. The white slowness vector $\mathbf{p}$ points to the maximum of $P(\omega, \mathbf{p})$. Its length resolves an apparent sound velocity of 350 m/s. An azimuth of 324 degrees is found as angle between $\mathbf{p}$ and the North.

6.2.3 Localization through cross-bearing

KNMI operates two experimental infrasound arrays in De Bilt (DBN) and Witteveen (WIT). Figure 6.6 shows the result of the cross bearing analysis. In a point source approach one expects the three bearings to cross in one point, the point of excitation. But rather than having a point source, a pressure wave is generated as a continuous plane wave during the supersonic flight. Furthermore, the meteorological parameters wind and temperature control the sound wave propagation. Therefore, a sonic boom is not necessarily recorded on more than one array. Azimuths are also influenced by the atmospheric conditions along the ray path. Therefore, the uncertainties in the source location can immediately be inferred from figure 6.6.

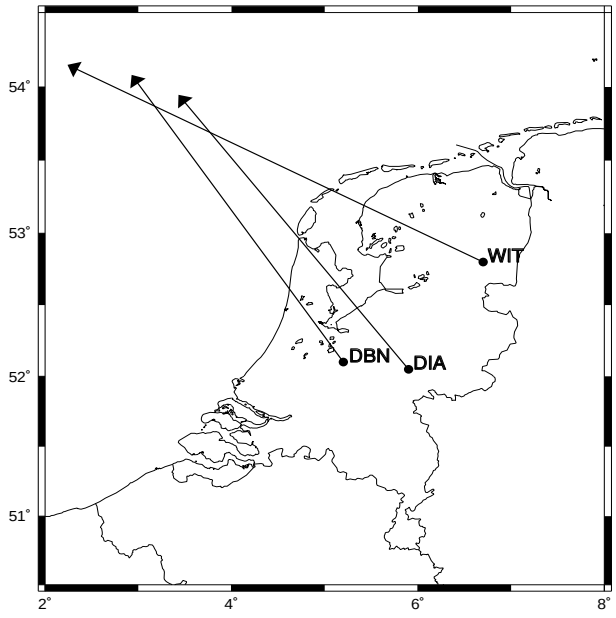

Figure 6.6: *Cross bearing*

6.3 An exploding meteor

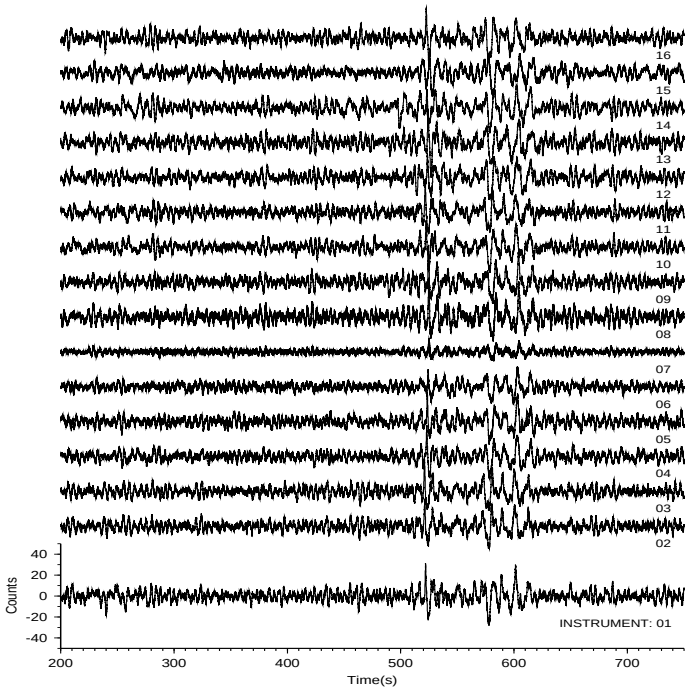

Figure 6.7: *Recordings from an exploding meteor*

In figure 6.7 coherent energy is detected between 500 and 600 seconds after 04h09m24.4s GMT on November 8th, 1999. To major arrivals separated approximately 50 seconds can be seen. Supported by human observations these waveforms are caused by an exploding meteor above Northern Germany at an estimated distance of 400 km from DIA. A meteor generates infrasound upon entering the earth's atmosphere at heights lower than 50 km (*Donn and Balachandran,* 1974) and (*McIntosh, Watson, and ReVelle,* 1976). Shock waves are produced when the meteor explodes, or thermally bursts, at a height of 20 km (*ReVelle,* 1975).Throughout the recording small packages of coherent energy, less in amplitude than the meteor's arrival, are visible, for example around 280 and 430 seconds. The so-called microbaroms are produced by the atmospheric coupling of standing ocean waves (*Posmentier,* 1967).

6.3.1 Frequency domain analyses

The top frame in figure 6.8 shows the best beam for the meteor, Fisher values are plotted in the middle frame and azimuths of the incoming energy in the lower frame. The best beam has an amplitude summed over the sixteen traces. Therefore, the average amplitude of the first arrival from the meteor is the best approximation for the generated pressure variation. This corresponds to a value of 0.75 Pa (see Appendix B). The Fisher value as a measure of the signal coherency, increases over a large range of frequencies at the meteor arrival time, after 510 seconds. The secondary arrival after 560 seconds has a lower frequency contents of 0.1 Hz. Its differential traveltime of 50 seconds and damped higher frequency part indicate a thermospheric reflection (*Garcés, Hansen and Lindquist,* 1998).

On the other hand, microbarom coherency is bounded to smaller frequency ranges, showing up through the whole record. The coherency of the meteor signal is also reflected when evaluating the azimuth as plotted in the lower frame. The meteor energy is coming from the North-east, while yellow to red colors indicate a North-western origin for the microbarom energy. From figure 6.8 it follows that the first arrival of the meteor has

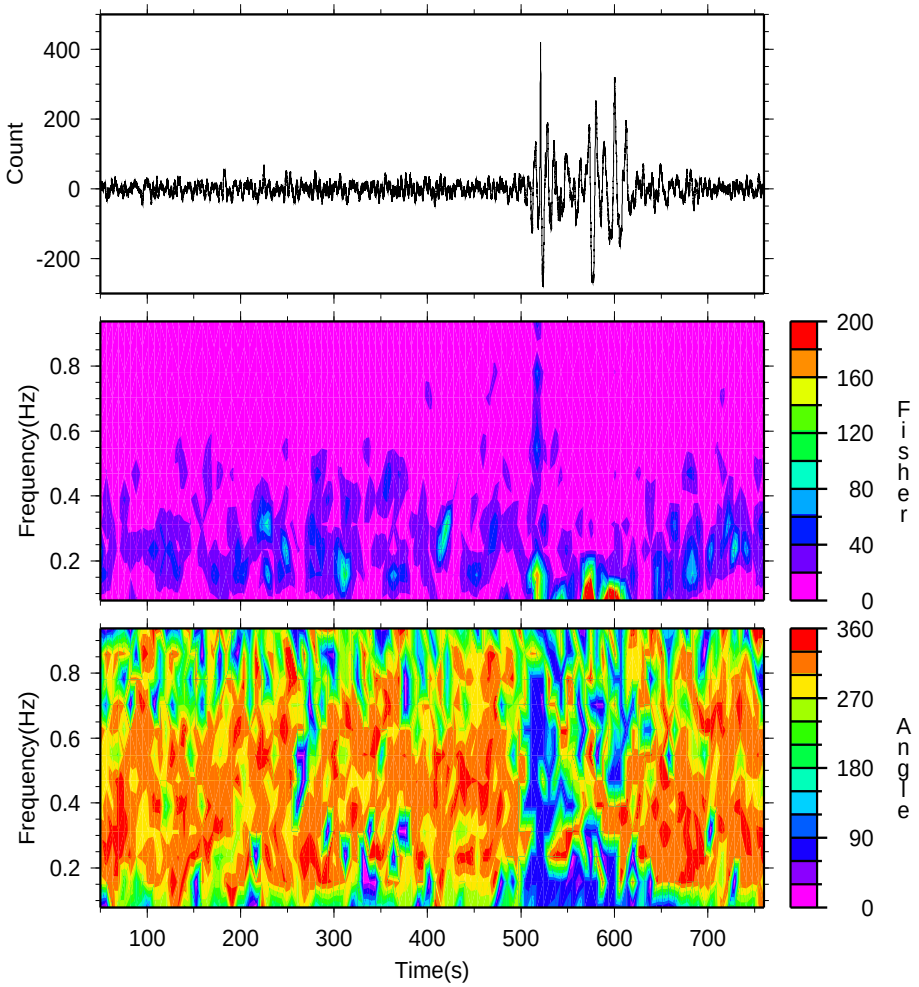

Figure 6.8: *Best beam and coherency*

maximum Fisher values, i.e. coherency, around 0.15 Hz. The power of the f-p spectrum $P(\omega, \mathbf{p})$ is calculated for a frequency of 0.15 Hz. Figure 6.9A shows the result for this calculation. The detected energy is characterized by a velocity c of 353 m/s coming in with an angle ϕ of 81.9 degrees. Some microbaroms energy is present in the North-western quadrant.
A large Fisher value for the microbaroms is found around 310 seconds in figure 6.8. The coherent energy is centralized around 0.19 Hz. Locating this energy is done in figure 6.9B. The microbarom energy is characterized by a velocity c of 390 m/s and ϕ 309 degrees. Comparing the apparent sound velocities of the different events, implies a steeper angle of incidence for the microbarom energy. Although detailed ray-tracing will resolve the propagation paths, the microbarom energy is likely to propagate to higher atmospheric altitudes resulting in a steeper incoming angle.

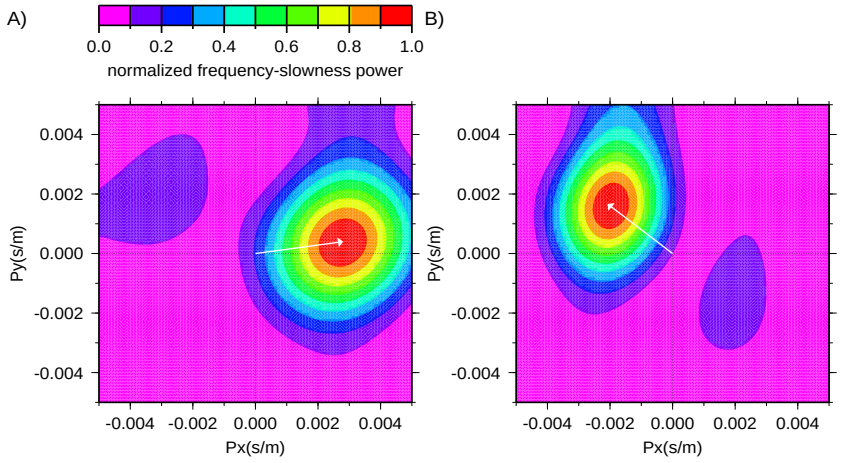

Figure 6.9: *Frequency-slowness analysis. A) The 0.15 Hz component of the meteor. B) The 0.19 Hz component of the microbaroms.*

6.3.2 Interpretation

Standing wave patterns on the sea surface, generated by storm centers, produce infrasonic waves in the atmosphere (*Wilson,* 1981). Based on theory for microseism described by (*Longuet-Higgens,* 1950), (*Posmentier,* 1967) concluded that the compressibility of air has no significant effect on the pressure fluctuations. Therefore, microseism and microbaroms are generated by standing ocean waves, with an oscillatory pressure of:

$$P = -2\rho_0 a^2 \omega^2 cos2\omega t \tag{6.11}$$

where, ρ_0 is the density of air in the microbarom case and of water for microseism, a the amplitude of the standing wave with frequency ω at time t. In figure 6.10 the pressure amplitudes of $a^2\omega^2$ are plotted, calculated from oceanic wave data. Furthermore, the resolved azimuthal angles of DIA are denoted by the vectors. The $a^2\omega^2$ data were obtained at 06h00m GMT. The wave period of the maximum is 9.8 seconds. By making use of equation 6.11, a pressure variation of 0.2 Hz is induced. This correlates with the 0.19 Hz found in the frequency domain analyses. A possible explanation for the discrepancy between the observed azimuth and location of the maximum can be found in the source of the data. P describes the generated pressure due to standing ocean waves, while the contours in figure 6.10 result from wave patterns as such. Wave interference, generating standing waves, occurs close to an atmospheric depression but does not necessarily coincide with $a^2\omega^2$ maximum derived from non standing ocean waves. Furthermore, the atmospheric depression and associated meteorological temperature and wind profiles nearby, will heavily influence the sound propagation and possibly deflect the acoustic waves (*Ørbæk and Naustvik,* 1995).
Infrasound from the meteor originates North-east of DIA. The location above Northern Germany is confirmed by human observations. According to (*ReVelle and Delinger,* 1981), based on a high frequency extrapolation of the Lamb wave results (*Lamb,* 1902) and (*Lamb,* 1910), the energy of the exploding meteor can be obtained from:

$$\frac{\Delta p r^{1/2}}{E} = 2.34 \cdot 10^3 T^{-1.5} \tag{6.12}$$

where, Δp is the peak to peak amplitude of the first cycle waveform, r is the horizontal distance range from source to observer, E is the total energy release and T is the period of the first cycle of the Lamb wave. Thus, the total amount of energy released by the exploding meteor, taken a distance of 400 km, equals: 1.1 kT TNT or $4.6 \cdot 10^{12}$J.

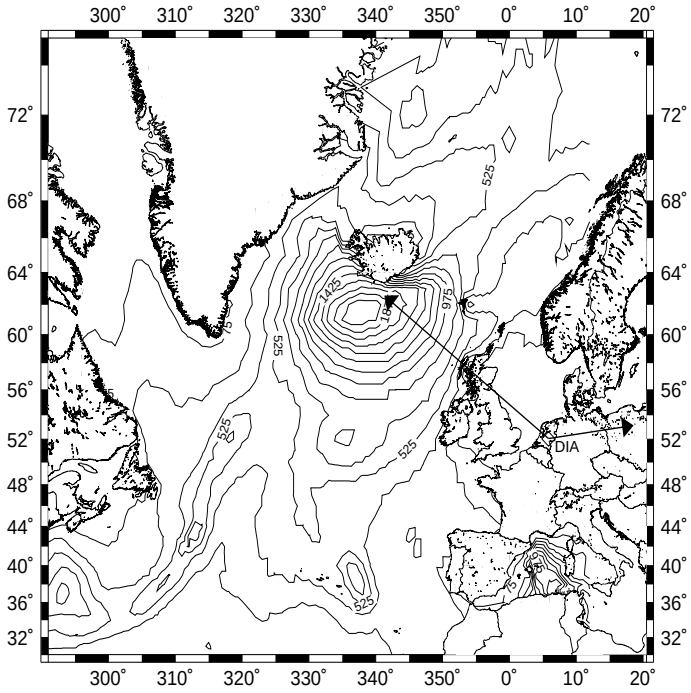

Figure 6.10: *Resolved azimuths by DIA and pressure amplitude contours of $a^2\omega^2$ (in m^2s^2) of infrasound generated by ocean waves*

7 Conclusion

7.1 Conclusions

KNMI has been able to show that sonic booms can be detected and localized using a micro-barometer array. For this purpose, the KNMI micro-barometer was developed (responding to events between 0.002 and 30 Hz). A detection and localization algorithm based on frequency-wavenumber analysis including Fisher statistics, proved to be a low threshold detector. Using data from two experimental arrays leads to an accurate position of the source through cross bearing.

7.2 Recommendations

As described, the signal detection algorithm and other array processing are based on signal coherency (or, signal correlation in time domain procedures). It is shown that signals traveling over the array are coherent, otherwise the Fisher detector would not work. On the other hand, signal coherency does not imply a flat wave front (plane wave) for the pressure variations. The basis of most techniques is however the assumption of dealing with a plane wave. Better understanding of the shape of the wave front will lead to more accurate detection and localization. This better understanding can be achieved by obtaining more knowledge about: how infrasonic waves travel through the air and what influences their wave-shape. Two major physical parameters which influence the behavior of infrasonic waves are: wind speed and temperature. These quantities can be measured and an atmospheric model can be created. Ray-tracing through the model will show the behavior of a pressure wave through the atmosphere (*Garcés, Hansen and Lindquist,* 1998). Reflections and refraction will show up and explain part of the complex forms of the measured waves. Focusing effects, which severely increase the intensity, can be resolved and even predicted depending on the atmospheric conditions.

Frequency-wavenumber spectrum analyses in a statistical approach is one way to detect signal. A wide variety of time (p.e. (*Cansi,* 1995)) and frequency domain based detectors are developed or can be thought of. To compare these detectors on performance with respect to reliability and computing time, will give more insight in the (dis)advantages of a specific detector. A set of efficient and low threshold detectors, which can be chosen from depending on the application, will enhance the understanding of acoustic wave propagation.

Source detection can be achieved by solely measuring the arrival times of the first incoming wave per instrument. However, infrasonic waves contain much more information which, for example, can be resolved through ray-tracing (see recommendation above). The wave shape is amongst others described by the amplitude. Amplitude information can be used to extract information of the explosive intensity of the source. In case of reflections, amplitude information will give the amount of energy reflected and transmitted on the reflective surface. The KNMI micro-barometer measures amplitude in Volts, induced by a deflection of the diaphragm. Reliable estimates of how the Volts are correlated to physical pressure values (p.e. Pa or bar), are available. However, to work properly with the highly sensitive instrument is of great importance to do an exact calibration of each instrument individually. Applying pressure variations with known amplitude and frequency to the instrument, will resolve its response characteristics.

References

Cansi, Y., An automatic seismic event processing for detection and location: The P.M.C.C. method, *Geoph. Res. Lett., 22,* 1021-1024, 1995.

Donn, W.L., and N.K. Balachandran, Meteors and meteorites detected by infrasound, *Science, 185,* 707-709, 1974.

Garcés, M.A, R.A. Hansen, and K.G. Lindquist, Traveltimes for infrasonic waves propagating in a stratified atmosphere, *Geoph. J. Int., 135,* 255-263, 1998.

Haak, H.W., An acoustical array for subsonic signals, *Tech. Rep. WR 96-03,* 22 pp., Royal Neth. Meteo. Inst., de Bilt, the Netherlands, 1996.

Haak, H.W. and G.J. de Wilde, Microbarograph systems for the infrasonic detection of nuclear explosions, *Tech. Rep. WR 96-06,* 45 pp., Royal Neth. Meteo. Inst. (KNMI), De Bilt, The Netherlands, 1996.

Lamb, H., On wave propagation in two dimensions, *Proc. Lond. math. Soc., 35,* 141-161, 1902.

Lamb, H., On atmospheric oscillations, *Proc. Lond. math. Soc., A84,* 551-572, 1910.

Longuet-Higgens, M.S., A theory of the origin of microseism, *Phil. Trans. of the Roy. Soc. of London, 243,* 1-35, 1950.

McIntosh, B.A., M.D. Watson, and D.O. ReVelle, Infrasound from a radar-observed meteor, *Canadian J. of Phys., 54,* 655-662, 1976.

Ørbæk, J.B, and M. Naustvik, Infrasonic signatures of a Polar Low in the Norwegian and Barents Sea on 23-27 March 1992, *Tellus, 47A,* 921-940, 1995.

Posmentier, E.S., A theory of microbaroms, *Geoph. J. of the Royal Astr. Soc., 13,* 487-501, 1967.

Preparatory Commission for the Comprehensive Nuclear-Test-Ban Treaty Organization *Comprehensive Nuclear-Test-Ban Treaty (CTBT),* 139 pp., V.97-28276, Austria, 1997.

ReVelle, D.O., Studies of sounds from meteors, *Sky and Telescope, 49,* 87-91, 1975.

ReVelle, D.O. and W.G. Delinger, Passive acoustic remote sensing of infrasound on natural origin, *Proc. Int. Sym. Acous. Rem. Sens. of the Atm. and Oceans, Calgary, Alberta, Canada,* 1981.

Smart, E., and E.A. Flinn, Fast frequency-wavenumber analysis and Fisher signal detection in real-time infrasonic array data processing, *Geoph. J. of the Royal Astr. Soc., 26,* 279-284, 1971.

Wilson, C.R., Atmospheric infrasound, *Antarctic J. of the U.S., 16,* 198-199, 1981.

8 Appendix A

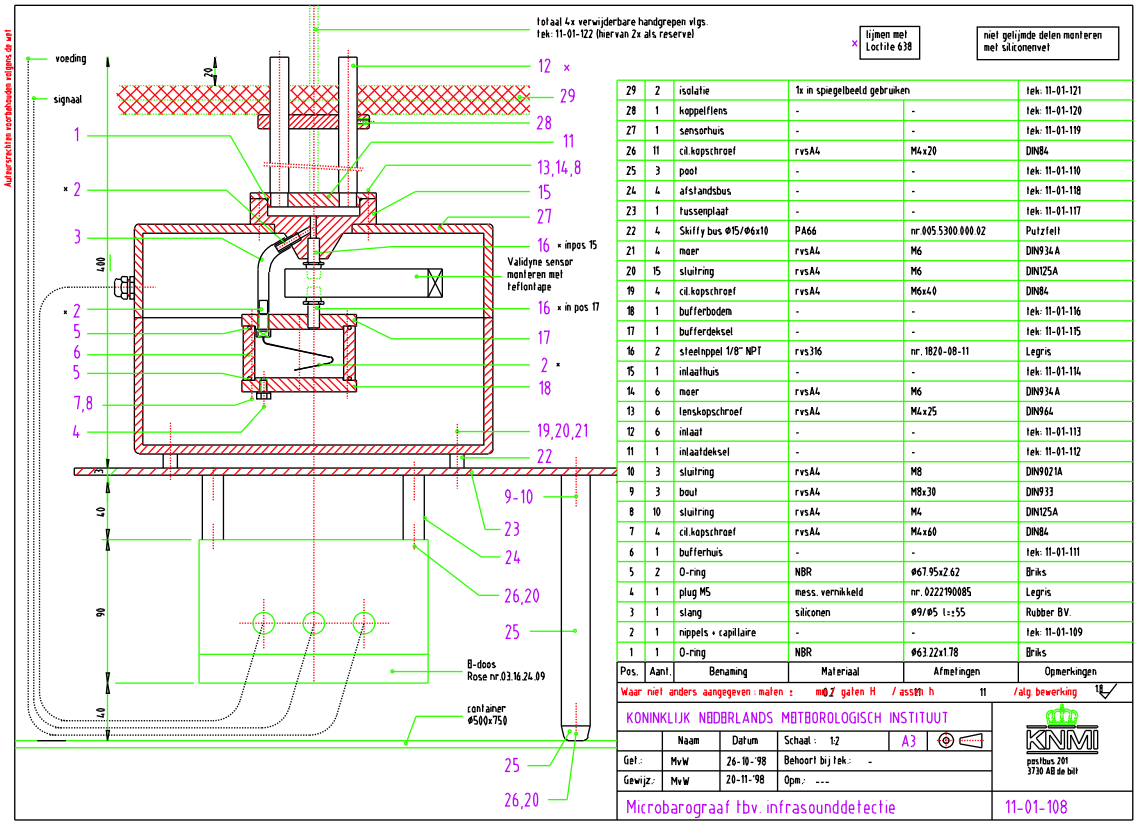

Pos.	Aant.	Benaming	Materiaal	Afmetingen	Opmerkingen
29	2	isolatie	1x in spiegelbeeld gebruiken		tek: 11-01-121
28	1	koppelflens	-	-	tek: 11-01-120
27	1	sensorhuis	-	-	tek: 11-01-119
26	11	cil.kopschroef	rvsA4	M4x20	DIN84
25	3	poot	-	-	tek: 11-01-110
24	4	afstandsbus	-	-	tek: 11-01-118
23	1	tussenplaat	-	-	tek: 11-01-117
22	4	Skiffy bus ø15/ø6x10	PA66	nr.005.5300.000.02	Putzfelt
21	4	moer	rvsA4	M6	DIN934A
20	15	sluitring	rvsA4	M6	DIN125A
19	4	cil.kopschroef	rvsA4	M6x40	DIN84
18	1	bufferbodem	-	-	tek: 11-01-116
17	1	bufferdeksel	-	-	tek: 11-01-115
16	2	steelnippel 1/8" NPT	rvs316	nr. 1820-08-11	Legris
15	1	inlaathuis	-	-	tek: 11-01-114
14	6	moer	rvsA4	M6	DIN934A
13	6	lenskopschroef	rvsA4	M4x25	DIN964
12	6	inlaat	-	-	tek: 11-01-113
11	1	inlaatdeksel	-	-	tek: 11-01-112
10	3	sluitring	rvsA4	M8	DIN9021A
9	3	bout	rvsA4	M8x30	DIN933
8	10	sluitring	rvsA4	M4	DIN125A
7	4	cil.kopschroef	rvsA4	M4x60	DIN84
6	1	bufferhuis	-	-	tek: 11-01-111
5	2	O-ring	NBR	ø67.95x2.62	Briks
4	1	plug M5	mess. vernikkeld	nr. 0222190085	Legris
3	1	slang	siliconen	ø9/ø5 l=±55	Rubber BV.
2	1	nippels + capillaire	-	-	tek: 11-01-109
1	1	O-ring	NBR	ø63.22x1.78	Briks

Waar niet anders aangegeven : maten ± ø0.2 gaten H / ass±th h 11 / alg. bewerking 18

	Naam	Datum	Schaal : 1:2	A3
Get.:	MvW	26-10-'98	Behoort bij tek.: -	
Gewijz.:	MvW	20-11-'98	Opm.: ---	

Figure 8.1: Constructional drawing of the KNMI micro-barometer

9 Appendix B

A calibration experiment has be done to get a measure of how Volts (and counts) correlate to pressure variation in Pascal (Pa). The experiment is performed in the following way: the KNMI micro-barometer is vertically displaced over a certain distance h. The pressure variation Δp through displacement equals:

$$\Delta p = \frac{F}{A} = \frac{mg}{A} = \frac{\rho_{air} V g}{A} = \rho_{air} g h \tag{9.1}$$

where, F is the applied force over a column air of area A. Then, m is the displaced mass of air with density ρ_{air} and volume V, g equals 9.81 m/s.

The micro-barometer is displaced over 2.9 meter; thus generating a pressure variation of:

$$\Delta p = 1.3 \cdot 9.81 \cdot 2.9 = 37 Pa \tag{9.2}$$

Several displacements resulted in an average output reading of 655 mV. The 16 bits A/D conversion ranges within ± 10 Volts between 0 and ± 32768 Counts. Thus:

$$1 \text{ mV} = 37/655 \text{ Pa and } 1 \text{ mV} = 3.2768 \text{ Counts}$$
$$\text{so,}$$
$$1 \text{ Count} = 0.01724 \text{ Pa}$$

10 Appendix C

Instr	Lon.(degr)	Lat.(degr)	X(m)	Y(m)
01	5.887803	52.061085	189296	452541
02	5.891335	52.059983	189539	452420
03	5.892850	52.058583	189644	452265
04	5.885016	52.050445	189113	451356
05	5.882173	52.050457	188918	451356
06	5.879316	52.050469	188722	451356
07	5.871658	52.058285	188191	452222
08	5.872492	52.059909	188247	452403
09	5.873623	52.061998	188323	452636
10	5.886852	52.056873	189234	452072
11	5.891101	52.054806	189527	451844
12	5.880589	52.058931	188803	452298
13	5.876988	52.060304	188555	452449
14	5.883257	52.056116	188988	451986
15	5.871691	52.055921	188195	451959
16	5.884049	52.063124	189037	452766
17	5.887978	52.061031	189308	452535

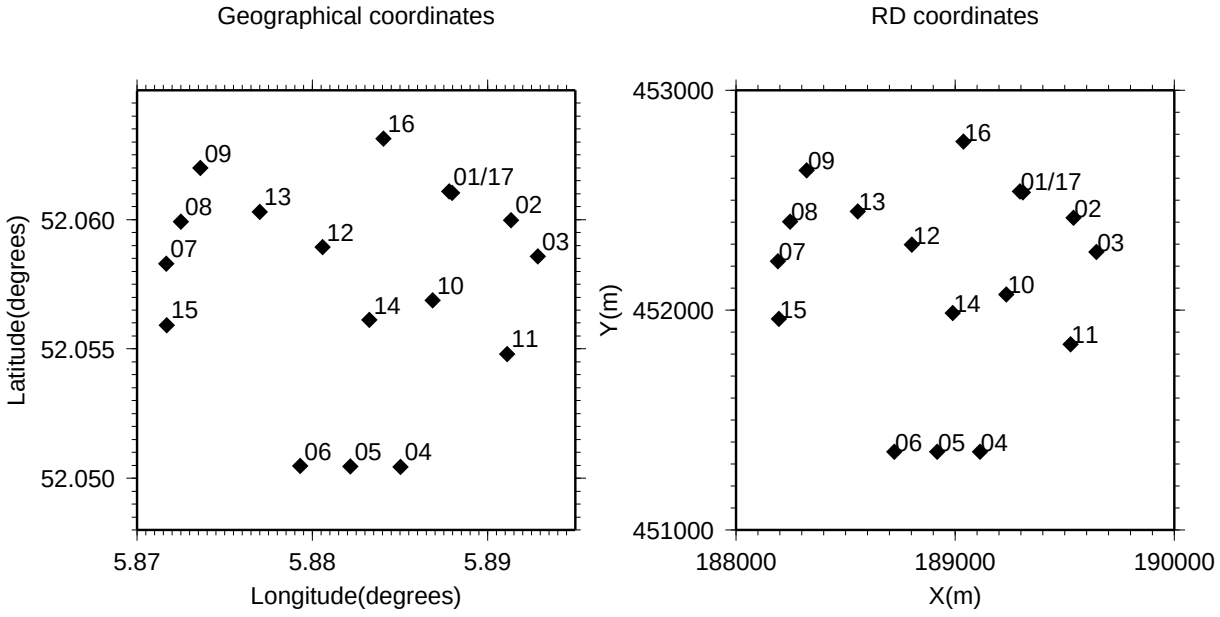

Figure 10.1: Exact coordinates of the array layout